ELSEVIER

Journal of Structural Geology 28 (2006) 745–761

JOURNAL OF STRUCTURAL GEOLOGY

www.elsevier.com/locate/jsg

A coupled micro- and macrostructural approach to the analysis of fluid induced brecciation, Curnamona Province, South Australia

Chris Clark [a,*], Andreas Schmidt Mumm [b], Alan S. Collins [a]

[a] *Continental Evolution Research Group, School of Earth and Environmental Sciences, University of Adelaide, S.A. 5005, Australia*
[b] *School of Earth and Environmental Sciences, University of Adelaide, Australia*

Received 29 October 2005; received in revised form 11 January 2006; accepted 21 January 2006
Available online 3 April 2006

Abstract

Conditions during the formation of breccias in the Curnamona Province (eastern South Australia) have been investigated through a detailed fractal, microstructural, structural and fluid inclusion study of the breccias, syn-tectonic quartz veins and surrounding rocks. Fractal analysis of clast shapes and clast size distributions were able to distinguish two styles of breccia and indicate that fluid pressure fluctuations played a significant role, though to differing degrees, in the initiation of the brecciation process. Approximate palaeostress orientations prevalent during brecciation and their relationship to the deformational history of the terrane have been reconstructed by combining the orientations of microfractures (sealed microfractures and fluid inclusion planes) with structural field data. Fluid pressure fluctuations of ~80 MPa during the brecciation process have been quantified by structurally constrained microthermometric analysis of syn-tectonic fluid inclusions coupled with an analysis of the metamorphic history of the area. Results from this study allow brecciation within the Curnamona Province to be placed within a structural framework and relate the process of brecciation to the interaction between regional hydrothermal alteration/fluid flow systems, shear zone formation and lithological contrasts within the upper crust during the Palaeoproterozoic Olarian Orogeny. These methods and findings provide a template for the study of brecciation processes in other terranes where fluid-induced brittle deformation is a controlling factor in the localisation of major ore deposits.

Keywords: Brecciation; Fluid pressure; Fractal analysis; Microstructure; Fluid inclusions

1. Introduction

The relationships between deformation history, fluid flow and brittle deformation in upper crustal settings has been the focus of numerous studies (e.g. Kerrich and Allison, 1978; Sibson, 1986; Laznicka, 1988; Oliver et al., 1990; Lorilleux et al., 2002) and many studies have attempted to constrain the magnitudes and orientations of the stresses involved in failure (Etheridge, 1983; Burnham, 1985; Valenta et al., 1994; Ord and Oliver, 1997; Cox et al., 2001; Oliver et al., 2001). Interest in the processes of brittle failure and brecciation related to elevated fluid pressures in the upper crust is because they are important factors in the control and localisation of many ore deposits (e.g. Reeve et al., 1990; Ridley, 1993; Genna et al., 1996; Lorilleux et al., 2002).

The Olary Domain in eastern South Australia (Fig. 1) is a Palaeoproterozoic terrane that contains numerous examples of brecciated rock, some associated with alteration and mineralisation, which have been shown to have a large degree of structural control (Yang and Ashley, 1994). Clark and James (2003) found that in addition to the broad structural controls, brecciation in the Curnamona Province occurred due to fluctuations in fluid pressure. Fluid pressure fluctuations were largely controlled by reverse faulting, related to compressional deformation, during the later stages of the Olarian Orogeny. However, the magnitudes of the fluid pressure fluctuations associated with failure have not been assessed. The Telechie Valley area, within the Olary Domain (Fig. 2), was selected as the site for study due to the extensive development of breccias, the variety of breccias present and the well-constrained structural setting of the area. The outcropping area allows the reconstruction of the structural geometry and its relationship to the brecciation to be deduced. The Telechie Valley area has also been the focus of a number of studies of fluid flow and fluid sources (Skirrow and Ashley, 2000; Kent et al., 2000; Payne, 2003; Clark et al., 2005).

* Corresponding author. Tel.: +61 8 83033174 53.
E-mail address: christopher.clark@adelaide.edu.au (C. Clark).

0191-8141/$ - see front matter © 2006 Elsevier Ltd. All rights reserved.
doi:10.1016/j.jsg.2006.01.005

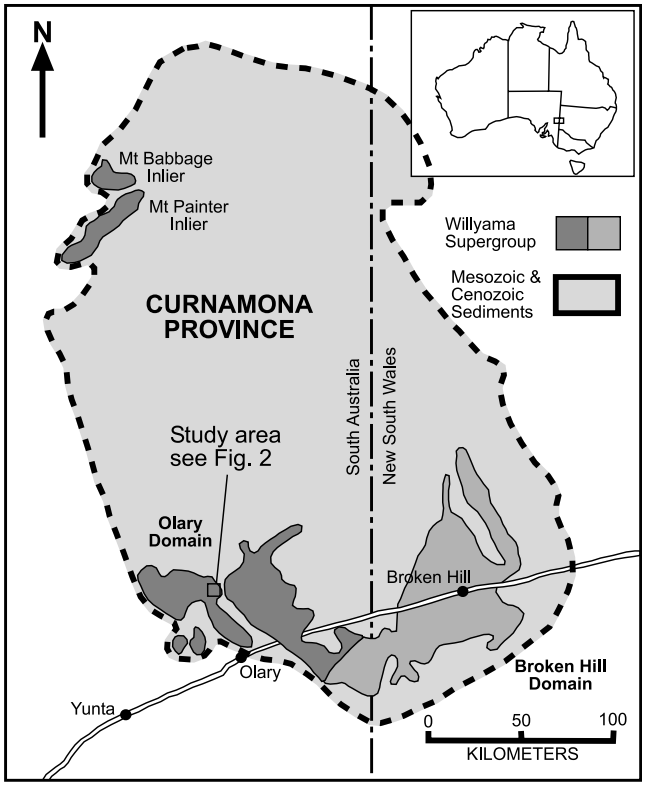

Fig. 1. Location map of the Olary Domain and Curnamona Province. The location of the study area within the Olary Domain is shown.

The first aim of this study is to determine whether the style of brecciation present in the area can be related to fluid pressure fluctuations. The second aim of the study is to constrain the palaeostress conditions that led to the formation of breccias and the magnitudes of the possible fluid pressure fluctuations. In order to achieve these aims, new fractal data on breccia clast shape and clast size distributions was acquired in order to quantify brecciation energies and style of breccias. The relationships between breccias and the host rocks have been deduced by mapping and fluid inclusion plane analysis of syn-tectonic quartz veins. Microthermometric analysis of fluid inclusions from within the fluid inclusion planes has been performed in order to characterise the PT conditions of fluid trapping during deformation.

2. Regional geology

The Olary Domain is a multiply deformed and metamorphosed Proterozoic terrane within the Curnamona Province of eastern South Australia (Fig. 1). Pelitic and psammitic metasediments of the Willyama Supergroup together with multiple generations of granitic and mafic intrusive bodies form the bulk of the exposed rocks in the area (Fig. 3). The tectono-metamorphic history of the Olary Domain is discussed by Clarke et al. (1986, 1987), Flint and Parker (1993), Robertson et al. (1998) and Gibson and Nutman (2004), and is only briefly discussed here. The earliest metamorphic-deformation cycle, D_1–M_1, resulted in syn-extensional, low pressure high temperature metamorphism and layer parallel S_1 fabric formation. It was also associated with bimodal magmatism at ca. 1.69 Ga (Gibson and Nutman, 2004). This was followed by the formation of D_2–M_2 recumbent folding and crustal thickening and the formation of a sub-horizontal to gently dipping S_2 fabric at 1.60 Ga (Gibson and Nutman, 2004). D_3–M_3 occurred at 1.58 Ga and involved NW–SE shortening to form NE-trending, upright F_3 folds and a penetrative, steep, NE-trending S_3 fabric and NE-trending retrograde shear zones (Flint and Parker, 1993). Peak metamorphism is inferred to have occurred at ca. 1.6 Ga (Page et al., 2000) and involved pressures of ca. 450 MPa following an anti-clockwise P–T path and increasing in grade from greenschist facies in the northwest to granulite facies in the southeast of the terrane (Clarke et al., 1987; Flint and Parker, 1993; Crooks and Webb, 2003). The second two (D_2–D_3) deformational cycles are attributed to the 1.60–1.58 Ga Olarian Orogeny (Page et al., 2000).

Several igneous suites have intruded the rocks of the Willyama Supergroup: A-type (Basso Suite) granitoids intruded at ca. 1.7 Ga and co-magmatic rhyolitic volcanic rocks erupted at ca. 1.71–1.70 Ga during deposition of the Willyama Supergroup (Ashley et al., 1996). This was followed by the intrusion of several mafic igneous masses and small I-type granitoid (Poodla and Antro Suites) bodies into the central part of the Olary Domain at ca. 1.64–1.63 Ga (Ashley et al., 1994). Following peak metamorphic conditions, voluminous S-type (Bimbowrie Suite) granitoids and associated pegmatites intruded the sequence. These are interpreted to be late syn-tectonic granites, which intruded at the end of the ca. 1.58 Ga D_3 event (Kent et al., 2000).

Further minor thermal perturbations occurred during the ca. 1100 Ma Musgravian Orogeny (Lu et al., 1996), mafic dyke emplacement during the development of the Adelaidean Rift Complex (ca. 820 Ma), and finally, two low-grade metamorphic/deformation events (D_4 and D_5) are attributed to the ca. 500 Ma Delamerian Orogeny (Flint and Parker, 1993). The Delamerian Orogeny also affected the Neoproterozoic Adelaidean sediments that overlie the Willyama Supergroup rocks. Paul et al. (2000) state that basement-involved deformation is linked to the reactivation of pre-existing structural anisotropies. Episodes of hydrothermal activity accompanied most of these later thermal events (Bierlein et al., 1995).

Fluid flow and associated brecciation in the Olary Domain has been the focus of a number of studies (Cook and Ashley, 1992; Yang and Ashley, 1994; Skirrow et al., 2000; Kent et al., 2000; Clark and James, 2003). These studies have proposed a hybrid magmatic–metamorphic source of fluids with an either syn- or post-orogenic timing for alteration. Kent et al. (2000) examined Sm–Nd isotope ratios of calcsilicate alteration and associated brecciation in the region and found that calcsilicate alteration occurred at 1575 ± 26 Ma. This age is consistent with Sensitive High Resolution Ion MicroProbe (SHRIMP) U–Pb ages of 1588–1583 Ma obtained on titanite from alteration assemblages and calcsilicate matrix breccias in the Telechie Valley (Skirrow et al., 2000) and also the timing of the Olarian D_3 deformational event. The origin of breccias in the Olary Domain has been discussed in earlier work (Cook and Ashley,

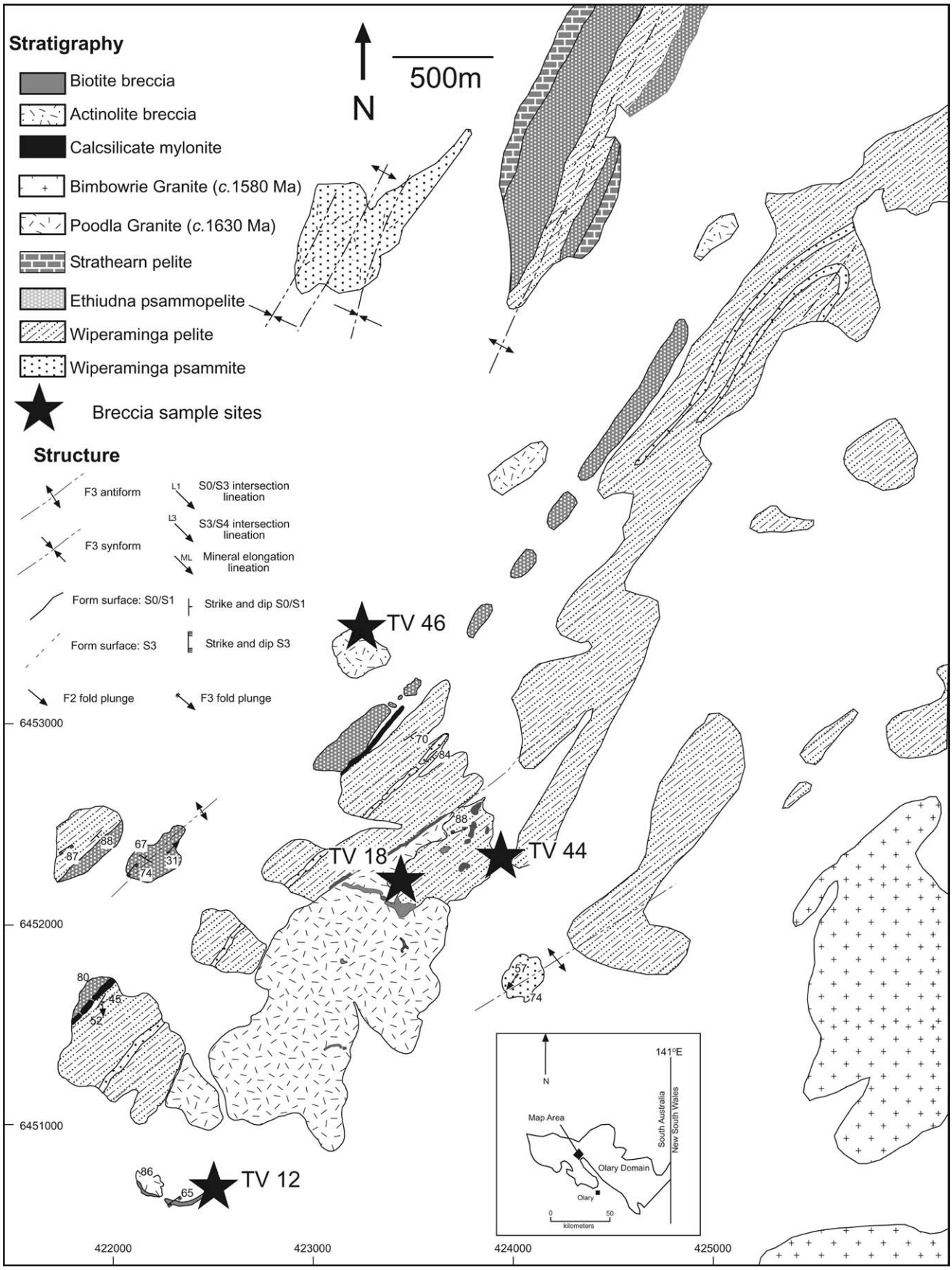

Fig. 2. Geological map of the Telechie Valley shear zone detailing the main structural elements and lithologies. The sample localities for the breccias used for fractal analysis are indicated by stars and the sample number.

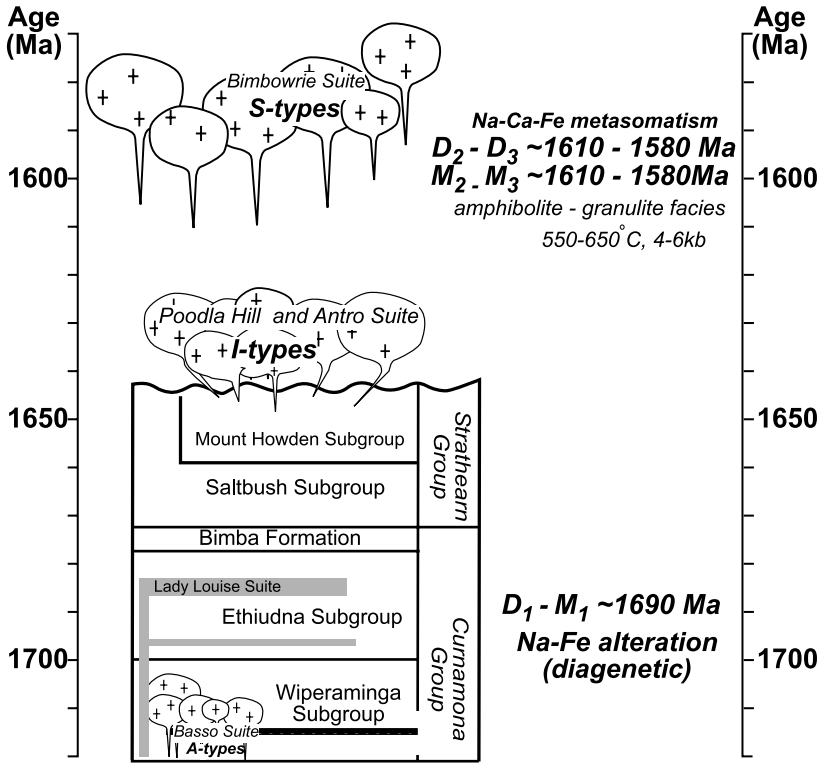

Fig. 3. Lithostratigraphic sequence of the Olary Domain incorporating major intrusive and tectonic events in the region (modified after Page et al., 2000).

1992; Yang and Ashley, 1994; Clark and James, 2003). Proposed brecciation mechanisms have ranged from diagenetic collapse (Cook and Ashley, 1992) to structural controlled failure during folding (Yang and Ashley, 1994) and fluid induced failure related to faulting (Clark and James, 2003). The location of the breccias in the Olary Domain show a degree of structural control as most are located in the cores of D_3 related folds or in D_3 high strain zones. This study focuses on two types of breccia associated with a D_3 high strain zone in the northern part of the Olary Domain; the Telechie Valley.

3. Methodology

Three main methods have been employed in this paper to describe and locate the approximate palaeostress vectors and quantify fluid pressure conditions associated with shearing and brecciation in the Telechie Valley area. They are: (i) field mapping and structural analysis; (ii) fractal analysis of clast morphology and size in the various breccias from the area; and (iii) microfracture orientation analysis combined with fluid inclusion microthermometry.

3.1. Mapping

Detailed mapping of breccia outcrops and major structural elements within the Telechie Valley area was undertaken at 1:5000 scale in order to establish the structural and lithological relationships of breccias with the host rocks. During mapping, oriented samples for fluid inclusion plane analysis and microthermometry were also taken.

3.2. Fractal analysis

Fractal analysis of breccias in the Telechie Valley was carried out on polished thin sections of a range of breccias from the studied area. High-resolution digital photomicrographs were taken at a constant magnification (×15) with a Nikon Coolpix 4500 at the highest possible resolution. The images were then adjusted in Adobe Photoshop v. 6.0 to enable the separation of clast and matrix. Image analysis of individual clasts was then performed using the image analysis program Scion Image (the windows version of the NIH-image program developed at the U.S. National Institute of Health). The dilation method of fractal analysis used for computing the clast morphology (D_r) is described in detail in Clark and James (2003). To ensure accurate measurements of clast morphologies only clasts with an area greater than 10000 pixels (equivalent to 0.0602 mm^2) were analysed (Berubé and Jébrak, 1999). A minimum of 30 clasts were analysed for each breccia to obtain significant fractal morphology histograms (FMH). The amplified fractal dimension, D_r^*, was used instead of D_r for better resolution on the FMH (Lorilleux et al., 2002).

The determination of the fractal representing the particle size distribution, D_s, was achieved by the digitisation of all visible clasts (273–523 clasts per sample) in a number of photomicrographs. Scion Image was then used to measure the areas of all clasts in the sample. Grain sizes, r, were then calculated as $\log(\sqrt{\text{grain area}})$ to conform to the method of Turcotte (1986). Earlier studies of fragmented rocks (Turcotte, 1986; Blenkinsop, 1991; Bjørnerud, 1998; Clark and James, 2003) have demonstrated that clasts sizes in breccias tend to

follow power-law relationships of the form $N_{(>r)}=Cr^{-b}$, where $N_{(>r)}$ is the number of clasts greater than size r and C and b are constants. The absolute value of b (the slope of the best-fit line on a log–log plot of $N_{(>r)}$ vs. r) is equivalent to the fractal dimension, D_s, of the particle size distribution (Turcotte, 1986). Care was taken to ensure all images used for D_s measurements were taken at the same magnification and the images used were of the same resolution so that comparisons between samples could be made. In calculating the value of D_s, a constant range of clast sizes (150–15000 pixels per clast, equivalent to 0.0025–0.0625 mm^2) was used in order to define the upper and lower fractal limits on D_s after the method suggested by Blenkinsop (1991).

3.3. Microstructural analysis and microthermometry

Microstructural analysis and fluid inclusion microthermometry were performed on doubly polished oriented thin sections approximately 100 μm thick. Microfracture and fluid inclusion plane (FIP) orientations were measured in oriented thin sections using a universal stage. To account for the inability of the universal stage measuring low dip FIPs (dips less than 45°), two orthogonal sections were cut and analysed for each sample and the results combined. Selected inclusions from FIPs representative of the stress conditions prevalent during shearing were then used for microthermometry. Primary fluid inclusions were also analysed in order to constrain the genetic fluid involved in the formation of quartz veins. Petrographic and genetic relationships were established according to the scheme of Roedder (1984).

Microthemometry on selected inclusions in known structural settings were analysed using a Linkam THMSG 600 heating and cooling stage. Measurements were taken via cycling, according to the method of Goldstein and Reynolds (1994) to attain accurate T_m and T_h measurements repeatable at a $\leq$0.1 °C error value. Eutectic temperatures were recorded via repeated measurements at rates of 5 °C/min.

4. Structural controls in the Telechie Valley

The Telechie Valley area is located in the northern part of the Olary Domain and is dominated by the northeast-trending structural fabric of the Telechie Valley shear zone and northeast-trending macro-scale folding (Fig. 2). The region displays evidence of four distinct structural events (D_1–D_4), with each phase associated with a defined set of structures. The timing of D_1 is currently the subject of some debate. Gibson and Nutman (2004) contend that D_1 and associated S_1 fabric development is related to an early 1690 Ma deformational event and assign D_{2-3} to the ca. 1610–1580 Ma Olarian Orogeny. In contrast, Flint and Parker (1993) contend that D_{1-3} structures are all related to the Olarian Orogeny and there is no earlier event. However, it is clear in the Telechie Valley that there is a layer parallel fabric (S_1) that has been subsequently folded by a number of later events (D_{2-4}). The final deformation in the Telechie Valley (D_4) is related to the ca. 500 Ma Late Cambrian Delamerian Orogeny (Robertson et al., 1998).

There are five dominant rock types within the Telechie Valley: pelites, psammopelites, psammites, granites, and breccias. The pelitic units in the shear zone are composed of muscovite + plagioclase + quartz with minor biotite. The psammopelites consist of a fine-grained aggregate of quartz + plagioclase + muscovite + biotite. In some places this unit has been sheared into a distinctive mylonite. The psammites consist of coarse-grained recrystallised quartz ribbons displaying undulose extinction within a fine-grained quartz and mica matrix. On the eastern side of the Telechie Valley (see Fig. 2) is the 1629 ± 12 Ma Poodla Granite (Cook et al., 1994) that is interpreted to have been structurally emplaced during D_3 associated shearing, i.e. between 1.61 and 1.58 Ga (Payne et al., 2003). There are two main types of breccia present in the Telechie Valley area: a biotite matrix breccia and an actinolite matrix breccia, both of which contain albitic clasts.

4.1. D_1 structures

The dominant fabric outside of the Telechie Valley shear zone is the bedding parallel S_1 fabric (Fig. 4a), which is associated with the D_1 deformational event (Flint and Parker, 1993). Regional scale F_2 and F_3 folding have subsequently folded this fabric. An early generation of quartz epidote veins (Fig. 5a) is associated with the layer parallel fabric. These deformed veins are best preserved in the hinge zones of later folds. No folding associated with this deformational event has been observed in the Telechie Valley.

4.2. D_2 structures

Rare examples of F_2 folds or fold hinges are seen refolded by the later D_3 shortening event (Fig. 5b). The F_2 folds in the area have shallow southeasterly dipping axial planes and sub-horizontal NNE-trending plunges. F_2 folds are tight to isoclinal in nature and, although tightened by the later D_3 event, they are assumed to have been originally tight.

4.3. D_3 structures

Structural elements relating to the D_3 event are the most prominent fabrics observed in the Telechie Valley. The D_3 event in the Telechie Valley is dominated by the development of a northeast-trending shear zone. The Telechie Valley shear zone has a well-developed sub-vertical shear foliation that has an average strike and dip of 039/84SE (Fig. 4b). Associated with this foliation is a strong mineral elongation lineation plunging 55° towards 239° (Fig. 4c). This lineation is defined by the alignment of biotite and in places the stretching of andalusite porphyroblasts (Fig. 5c). The shear zone formed under mid- to upper-greenschist facies conditions and is a zone of intense localised structurally-controlled fluid flow (Clark et al., 2005). Within the shear zone, early pegmatites form rare sigma-clasts and indicate a sinistral strike-slip component

associated with shearing (Fig. 5d). A set of sub-vertical SSE-trending fractures, with an average strike and dip of 116/86SW (Fig. 4d) are found consistently, and exclusively, within the shear zone. They exhibit a slight dextral offset and are interpreted to be antithetic shear fractures associated with D_3 shear zone formation.

Macroscopic F_3 folding of the S_1 fabric dominates the area outside the shear zone (Fig. 5e). Within the shear zone, F_3 folds occur in both the psammopelitic and the pelitic units. F_3 folds in the psammopelitic units are associated with a sub-vertical S_3 axial planar fracture cleavage (Fig. 4f). The orientations of folds in each lithology display different behaviours (Fig. 4e), with F_3 in the psammopelites generally having consistent plunges toward the northeast, well-correlated with the orientations of the S_3 axial planar fracture cleavage (Fig. 4f). In contrast, the orientations of the F_3 folds in the pelites define a stereonet girdle (Fig. 4e) with orientations ranging from northeast plunging to southwest plunging. There is also a slight difference in the trend of F_3 in the pelites to those observed in the psammopelites, with F_3 in the pelites being slightly more north–south oriented. These differences are interpreted to reflect variations in the behaviour of the psammopelitic and pelitic units to competency contrasts and strain partitioning between the two lithologies. F_3 in the pelites is rotated into parallelism with the finite-extension direction (parallel to the mineral elongation lineation) of the shear zone

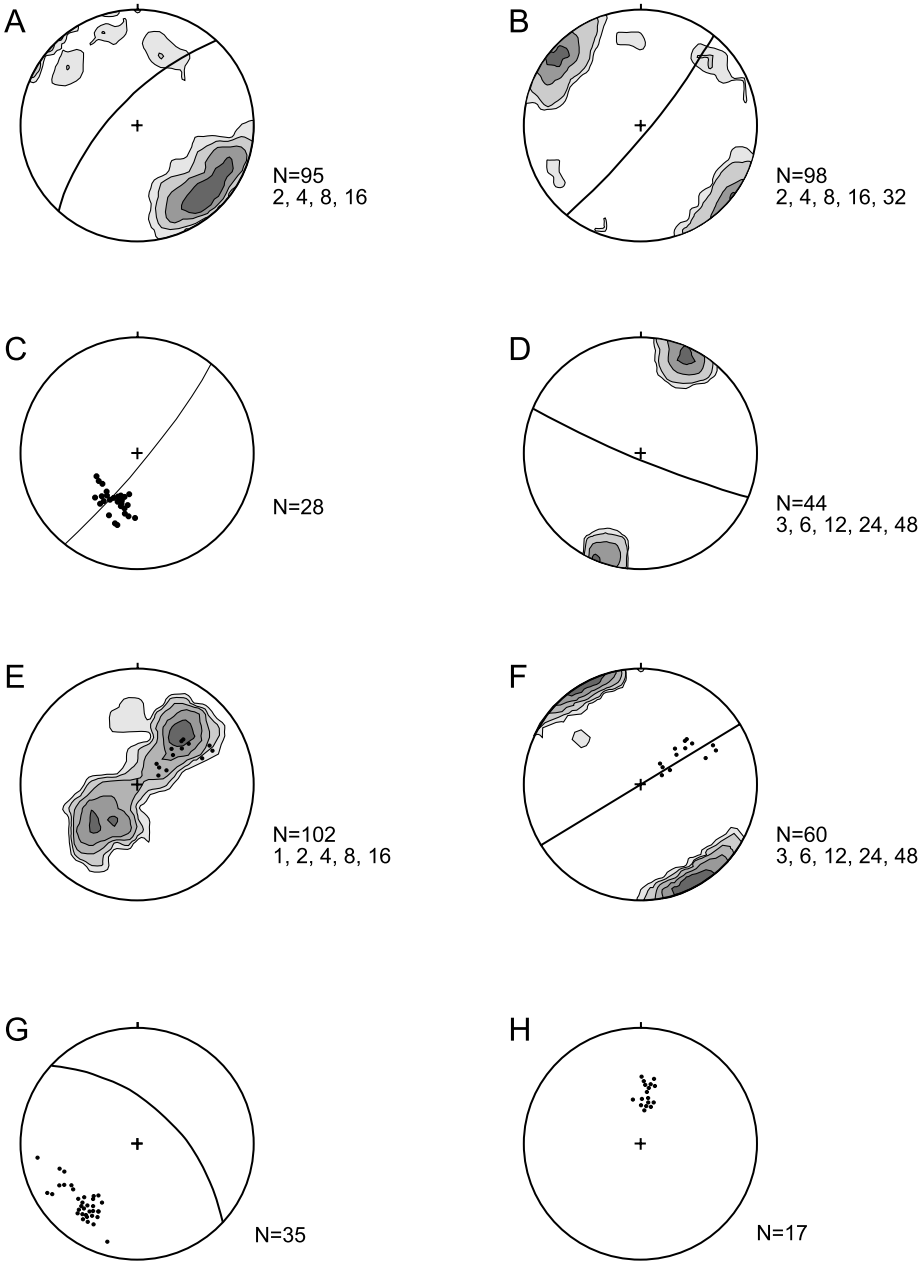

Fig. 4. Lower hemisphere equal area stereonets of major structural elements observed in the Telechie Valley: (A) poles to S_1 foliation surfaces, (B) poles to primary shear zone surfaces, (C) mineral elongation lineation data, (D) poles to antithetic fracture plane surfaces, (E) F_3 fold plunges showing the two plunge directions, (F) poles to S_3 cleavage planes, (G) poles of orientations of syn-D_3 quartz veins, and (H) F_4 fold plunges.

due to higher vorticity shearing in the less competent pelitic units, as documented elsewhere by other researchers (e.g. Bell, 1978; Carreras et al., 2005). The more competent psammopelitic units undergo shearing with a lower associated vorticity and therefore folding within these units does not undergo the same degree of rotation. This process of strain partitioning due to competency contrast between the different units results in the pelite F_3 fold plunges defining the observed girdle of rotation toward parallelism with the extension direction of the shear zone.

The rocks to the west of the shear zone are inferred to be overturned, whereas on the eastern side they are the right way up

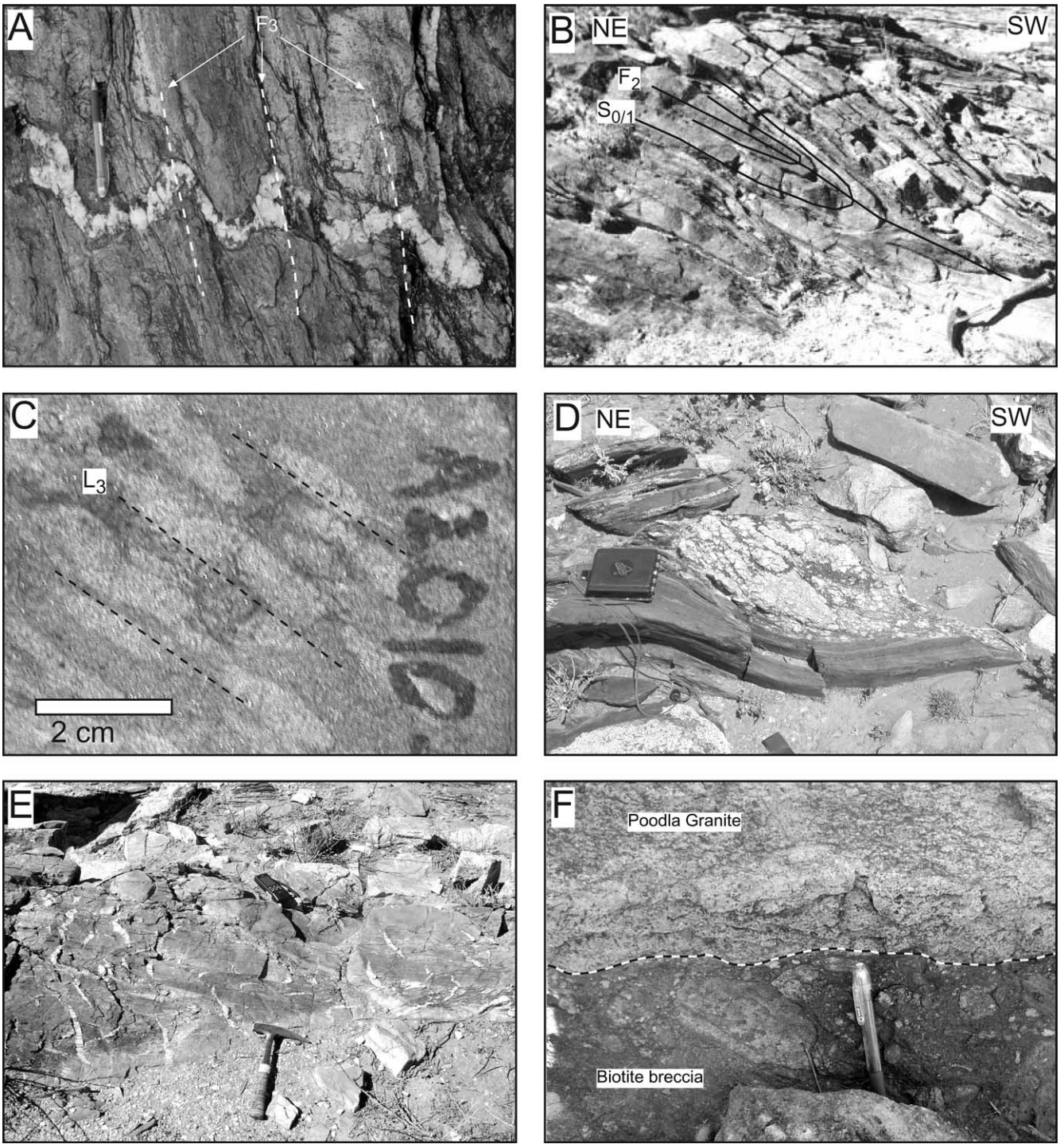

Fig. 5. Field photographs: (A) pre-D_3 quartz vein folded by upright F_3 folds looking NW (pen is 13 cm), (B) near isoclinal F_2 folding the bedding parallel S_1 fabric (hammer for scale ~40 cm), (C) elongated retrogressed andalusite porphyroblasts defining the stretching lineation related to D_3 shearing, (D) early pegmatite with winged tails (σ-clasts) indicating a sinistral sense of shear. This correlates to oblique reverse shearing (southeast over northwest), photo facing southeast (compass approximately 10 cm wide), (E) syn-D_3 quartz veins lying in the σ_1–σ_2 plane and opening in the σ_3 direction. Hammer for scale looking northeast, and (F) contact between the Poodla Granite and the biotite matrix breccias (pen is 13 cm).

(Conor, 2003). Regional mapping by Archibald (1980) interpreted the macro-scale structure and proposed that the overturning of lithologies was a result of regional scale nappe formation during the D_1 event. Gibson and Nutman (2004) have allied nappe formation to the D_2 event and suggested that the D_1 event was only responsible for the development of the layer parallel S_1 fabric and was not associated with fold generation. A generation of relatively undeformed quartz veins is related to the F_3 folds (Fig. 5e); these are interpreted to have formed during D_3 and are situated in the profile plane to the F_3 folds (Fig. 4g).

4.4. D_4 structures

Open north–south-trending, north plunging folds (Fig. 4h) that refold all previous structural fabrics are attributed to a D_4 deformational event. This event is most likely related to east–west compression during the post-Olarian Delamerian Orogeny. Minor, localised crenulation of the S_3 fabric is also interpreted to be a result of this event.

5. Brecciation in the Telechie Valley

Two main types of breccia are present in the Telechie Valley area. The classification of the two types is based on the matrix mineral assemblage, fractal characteristics of clast morphology, clast size distribution and contact relationship with the host rocks. The types recognised are: (1) a lithologically transgressive biotite breccia; and (2) an in-situ actinolite breccia.

5.1. Biotite matrix breccia

Breccias with rounded to sub-rounded albite + magnetite clasts in a matrix of biotite + quartz + albite + magnetite are found throughout the area (Fig. 6a and b). Clasts are generally less than 5 cm in diameter, with most clasts less than 1 cm. Biotite breccias are found to transgress bedding and lithological contacts in all rock types, but contain no local wallrock clasts (Fig. 5f). Widespread albitisation of many lithologies in the Olary Domain has been well documented (e.g. Cook and Ashley, 1992; Kent et al., 2000) and there is no way to be absolutely sure what the protolith to the biotite breccias were. It is clear that the granite wallrocks to these breccias are less intensely albitised (Fig. 5f) than the breccia clasts and therefore are unlikely to be the source of the breccia clasts. However, it is possible that the intensely albitised psammopelitic Ethiudna subgroup rocks present in the Telechie Valley shear zone are the source of breccia clasts.

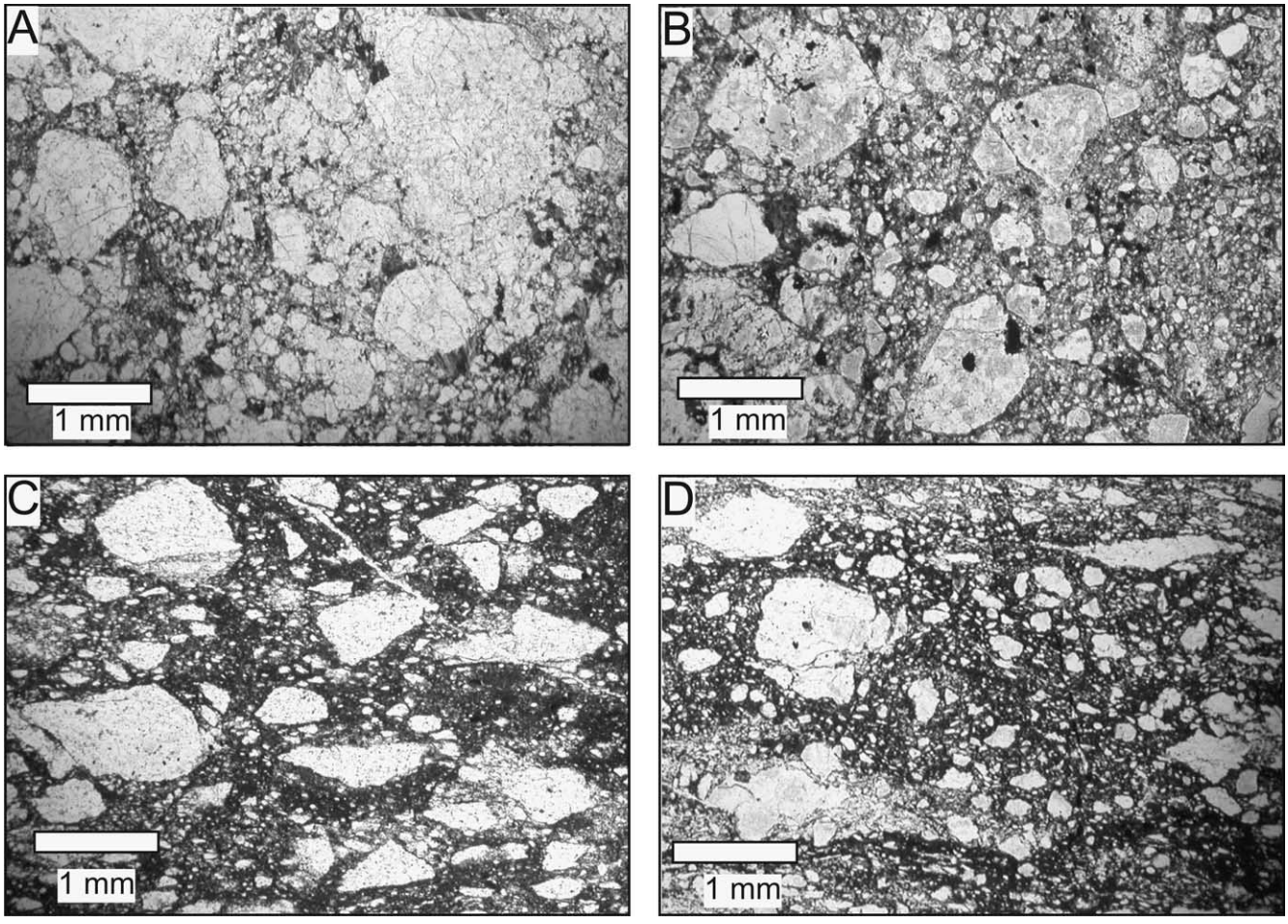

Fig. 6. Images of breccias used for fractal analysis: (A) TV12, (B) TV18, (C) TV44, and (D) TV46.

The biotite breccias are observed most commonly at the sheared margin at the contact between the Poodla Granite (Fig. 2) and the host metasediments with numerous breccia zones branching off into discrete fracture controlled zones that cross-cut the granite.

The biotite matrix breccias contain between 15 and 40 vol.% matrix and can be considered to be clast supported. Breccia clasts show little if any preferred clast orientation and the breccia matrix preserves no structural fabric. There is little compositional variation in the clasts although clasts of breccia are found in some areas indicating that there may have been multiple episodes of brecciation. Contacts between breccia and host rock are transgressive in nature and in general cut across the regional S_1 foliation indicating that breccia emplacement post-dated the early tectonic history of the area. The preferential use of the D_3 fabrics and structures indicates that brecciation is either contemporaneous with or post-dates D_3 deformation.

Fractal analyses of clast morphology (D_r^*) and particle size distribution (D_s) were performed on two samples (TV12 and TV18) of biotite breccia from different locations in the Telechie Valley. D_r^* values for sample TV12 (Fig. 7a), a biotite breccia from the southern contact of the granite and metasediments, vary between 3.4 and 7.3 with a Tukey's biweighted mean value of 4.47 ± 0.23 (30 clasts) and a D_s value of 1.33 (523 clasts) (Fig. 8a). Analysis of TV18, a biotite breccia from an intrusive breccia pipe at the northern end of the granite, yielded D_r^* values between 3.9 and 9.3 with a Tukey's biweighted mean of 5.59 ± 0.5 (Fig. 7b) and a D_s value of 1.34 (520 clasts) (Fig. 8b).

5.2. Actinolite breccia

Actinolite matrix breccias are characterised by angular to sub-rounded albite + quartz clasts supported by an unfoliated, coarse-grained matrix of actinolite + quartz + albite + apatite + clinopyroxene ± magnetite. Clasts vary from less than a centimetre up to several metres in diameter. The clasts are generally randomly oriented within the breccia matrix but in some cases show a degree of preferential alignment with the surrounding shear fabric. Actinolite matrix breccias most commonly occur within the albitised psammopelitic units of the Ethiudna subgroup within the Telechie Valley and show a large degree of in-situ development with jigsaw textures and gradation into unbrecciated wallrock commonly observed. In some locations breccia clasts contain a structural fabric; this fabric is interpreted to be the early layer parallel S_1 fabric. The location of the breccias within the core of the D_3 shear zone in the Telechie Valley indicates that brecciation and D_3 shearing are temporally and spatially related events.

Two samples of the actinolite breccia (TV44 and TV46) from different outcrops were used for fractal analysis (Fig. 6c and d). D_r^* values for sample TV44, an actinolite breccia from the northern end of the Poodla Granite, vary between 5.2 and 11.2 with a Tukey's biweighted mean value of 7.04 ± 0.46 (Fig. 7c) and a D_s value of 1.201 (273 clasts) (Fig. 8c). Analysis of TV46, an actinolite breccia from within the Telechie Valley

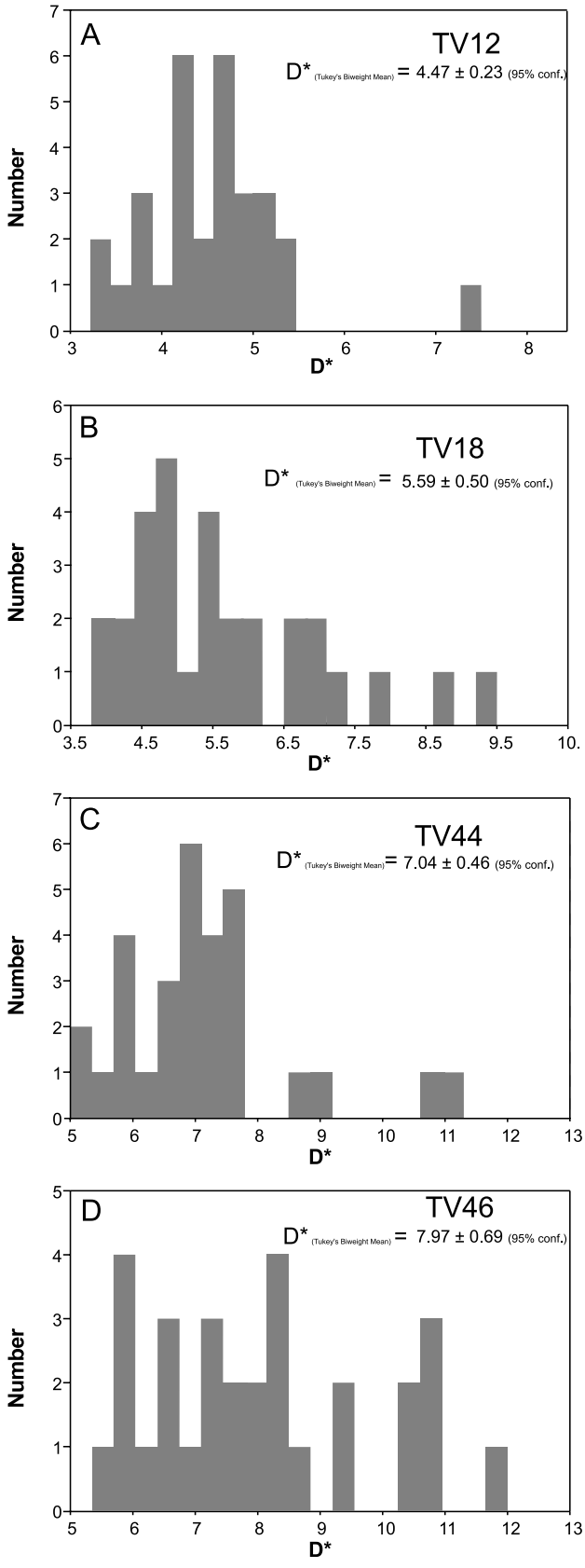

Fig. 7. Fragment morphology histograms (FMH) for the four breccias analysed: (A) TV12, (B) TV18, (C) TV44, and (D) TV46.

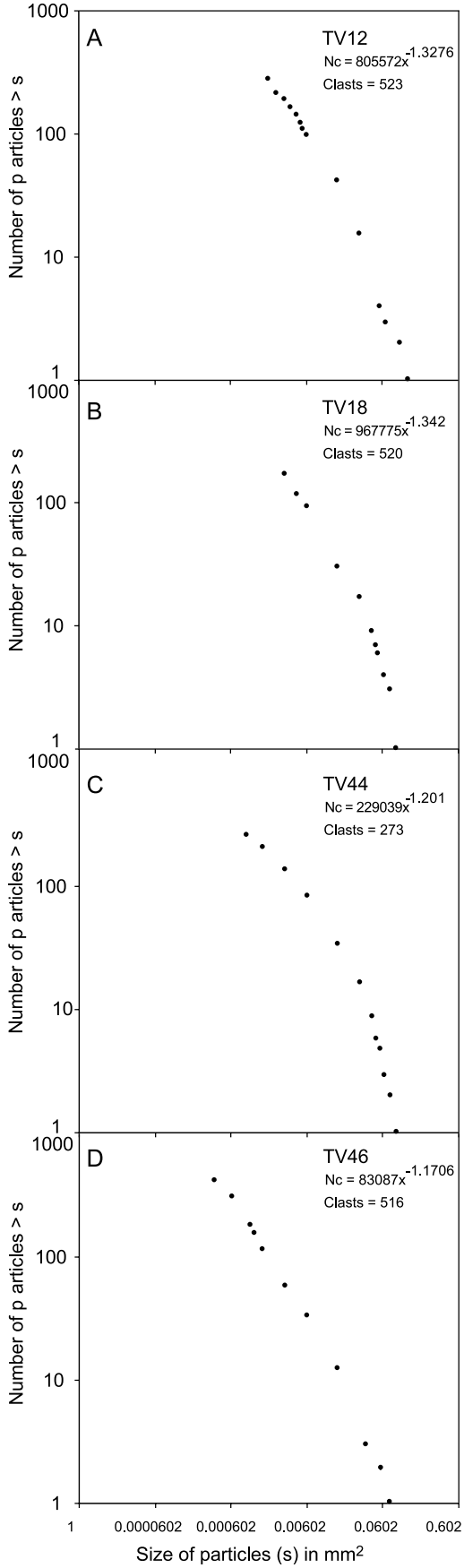

Fig. 8. Fractal dimension of size distribution of clasts sizes for the four breccias analysed: (A) TV12 biotite breccia, (B) TV18 biotite breccia, (C) TV44 actinolite breccia, and (D) TV46 actinolite breccia.

shear zone, yielded D_r^* values between 5.6 and 11.9 (Fig. 7d) with a Tukey's biweighted mean of 7.97 ± 0.69 (30 clasts) and a D_s value of 1.17 (516 clasts) (Fig. 8d).

6. Microfracture and fluid inclusion plane analysis

Microfracture and fluid inclusion plane analysis was performed on oriented samples of five different quartz veins from within the Telechie Valley shear zone and 259 measurements were recorded (Fig. 9a). The quartz veins sampled were virtually undeformed (e.g. Fig. 5e), and are interpreted to have formed during D_3 as they are found exclusively within the shear zone. The undeformed nature of the veins suggests that they formed at a late stage in the history of the shear zone. These veins are inferred to have opened during shearing in the extension direction of the shear zone and be related to fluid flow during the D_3 shearing event. Stable isotopic investigations of these veins have demonstrated that they formed at temperatures between 396 and 426 °C (Clark et al., 2005). Two types of microfractures were observed; fractures that contained few or no fluid inclusions (sealed microfractures) (Fig. 10a) and fractures that contained numerous fluid inclusions (fluid inclusion planes) (Fig. 10b). Microfracture orientations can be separated into four orientations. The four dominant strikes and dips observed were (i) 066/62 SE, 068/69 NW (Fig. 9b), (ii) 011/79 ESE (Fig. 9c), and (iii) 133/63 NE (Fig. 9d). The first three orientations consist of sealed microfractures (Fig. 9b and c) and in the fourth orientation microfractures dominantly consist of fluid inclusion planes (FIP) (Fig. 9d). These fracture orientations are consistent with having formed in the inferred D_3 stress field (see below).

7. Fluid inclusion microthermometry

Fluid inclusions trapped within the FIP in syn-tectonic quartz veins can be distinguished on the basis of the phase(s) observed at room temperature. According to this scheme two main types of fluid inclusion are present in all the samples collected and analysed: (i) two-phase liquid vapour inclusions (Fig. 10c) and (ii) three-phase liquid–vapour–solid (halite crystal) (Fig. 10d). The microthermometric results are summarised in Table 1.

Two-phase inclusions: water rich inclusions containing a single-phase vapour bubble (Fig. 10c). They are the dominant type of inclusion observed, accounting for over 80% of all inclusions present. Two-phase inclusions analysed in this study are found in FIPs of all orientations, they are also observed to occur as single inclusions in quartz crystals. These single inclusions are interpreted to be primary inclusions and represent the quartz vein forming fluid. Final melting of the ice phase occurred between −19.6 and −25.1 °C indicating inclusions contain between 22.4 and 26.1 wt% NaCl equivalent. On heating, vapour homogenisation temperatures for the two-phase inclusions were found to be in the range of 170–209 °C; these homogenisation temperatures are uncorrected for pressure.

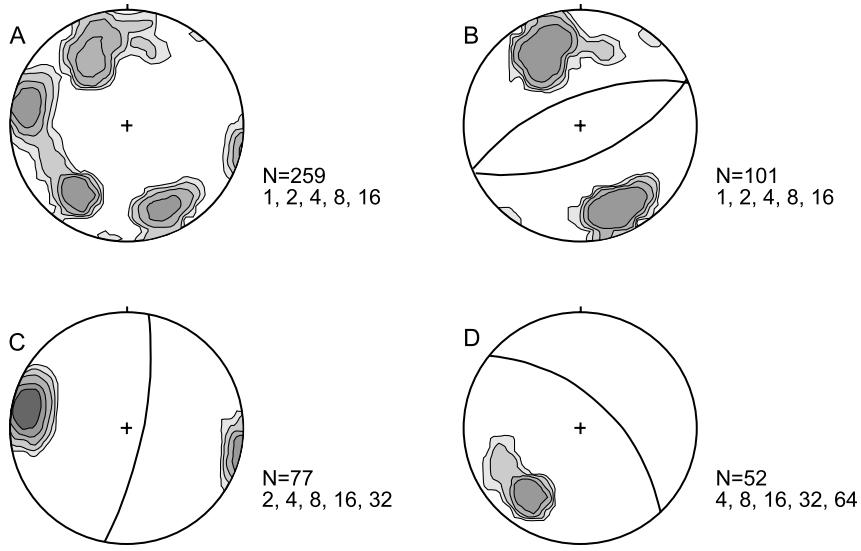

Fig. 9. Lower hemisphere equal area stereonets of the orientation of sealed microfractures and fluid inclusion planes (FIPs) from syn-tectonic quartz veins in the Telechie Valley: (A) combined orientations for all sealed microfractures and FIPs, (B) sealed microfractures in the same orientation as the shear plane, (C) sealed microfractures in an orientation expected for synthetic shear fractures, and (D) orientations of FIPs.

Three-phase inclusions: the three phase liquid–vapour–solid inclusions (Fig. 10d) are higher salinity fluids, with final melting of ice occurring at between −34.2 and −43.8 °C, representing salinities of 35.2–45.1 wt% NaCl equivalent (Yanattieva, 1946). Three-phase inclusions tend to form larger secondary inclusions compared with the two-phase inclusions. The eutectic temperatures indicate a composition dominated by bivalent cations (e.g. Ca^{2+}) with minor monovalent cations (e.g. Na^{+}) (Roedder, 1984). Vapour homogenisation temperatures of three-phase inclusions range from 217 to 246 °C (uncorrected for pressure). Solid dissolution in the three-phase inclusions consistently occurs at lower temperatures than vapour homogenisation (~150–160 °C) indicating that the original fluid was hypersaline, which is in agreement with previous studies of fluids inclusions from the same region (Kent et al., 2000).

8. Palaeostress and fluid pressure controls on breccia formation

8.1. Modes of brecciation

The styles of brecciation found in the Telechie Valley can be deduced by a combination of their structural setting, nature of their contact relationships with host lithologies and their fractal characteristics. This method was previously used to determine the style of brecciation in other areas (Jébrak, 1997; Lorilleux et al., 2002; Clark and James, 2003).

Biotite matrix breccias always exhibit a strong cross-cutting relationship with the Poodla Granite. This discordant relationship between breccia and the wallrocks suggests brecciation is intrusive in nature and has not developed in-situ. The local development of 'clast in clast' textures is suggestive of reworking of previously brecciated material by later brecciation events. The results of the fractal analysis of the clast morphologies and clast size distributions from two biotite matrix breccias add further weight to the argument that the breccia underwent a degree of transport at relatively high energies. The D_r^* values for the two biotite breccias are relatively low, TV12 = 4.47 ± 0.23 and TV18 = 5.59 ± 0.5 (Fig. 7a and b). These low values indicate that clasts have a relatively simple shape and are close to being spherical. Previous studies (Jébrak, 1997; Lorilleux et al., 2002; Clark and James, 2003) of breccias have linked low D_r^* values with the degree of transport experienced by the breccia where the lower values are indicative of a large degree of transport and physical wear of the clasts after initial fragmentation (Jébrak, 1997). Two possible transport mechanisms to account for clast rounding and the resulting low D_r^* observed in the biotite breccias are: (1) clast abrasion during high velocity clast–clast and clast–wallrock collisions, possibly during the emplacement of the breccia as a fluidised flow; (2) a lower velocity abrasive wear during cataclasis and fault movement; and (3) a combination of both factors. To explore the degree each of these mechanisms contributed to the observed D_r^* factors such as D_s, structural position, matrix composition (i.e. crushed wallrock/clast fragments or hydrothermal minerals) and clast/matrix ratios must also be considered. The D_s values obtained for the two samples are nearly identical (TV12 = 1.33 and TV18 = 1.34) and are greater in magnitude than the D_s values obtained (1.17–1.20) for actinolite matrix breccias. This could largely be due to a higher degree of transport of clasts resulting in particle size reduction leading to a greater abundance of finer particles. This process would result in higher values for D_s in the biotite breccias. Given the preferential location of the biotite breccias at the sheared margin of the granite (Fig. 2), breccia formation and emplacement was most likely synchronous with the D_3 shearing during the structural emplacement of the granite. Supporting this observation is the low matrix to clast ratio of the biotite breccias; previously this feature has

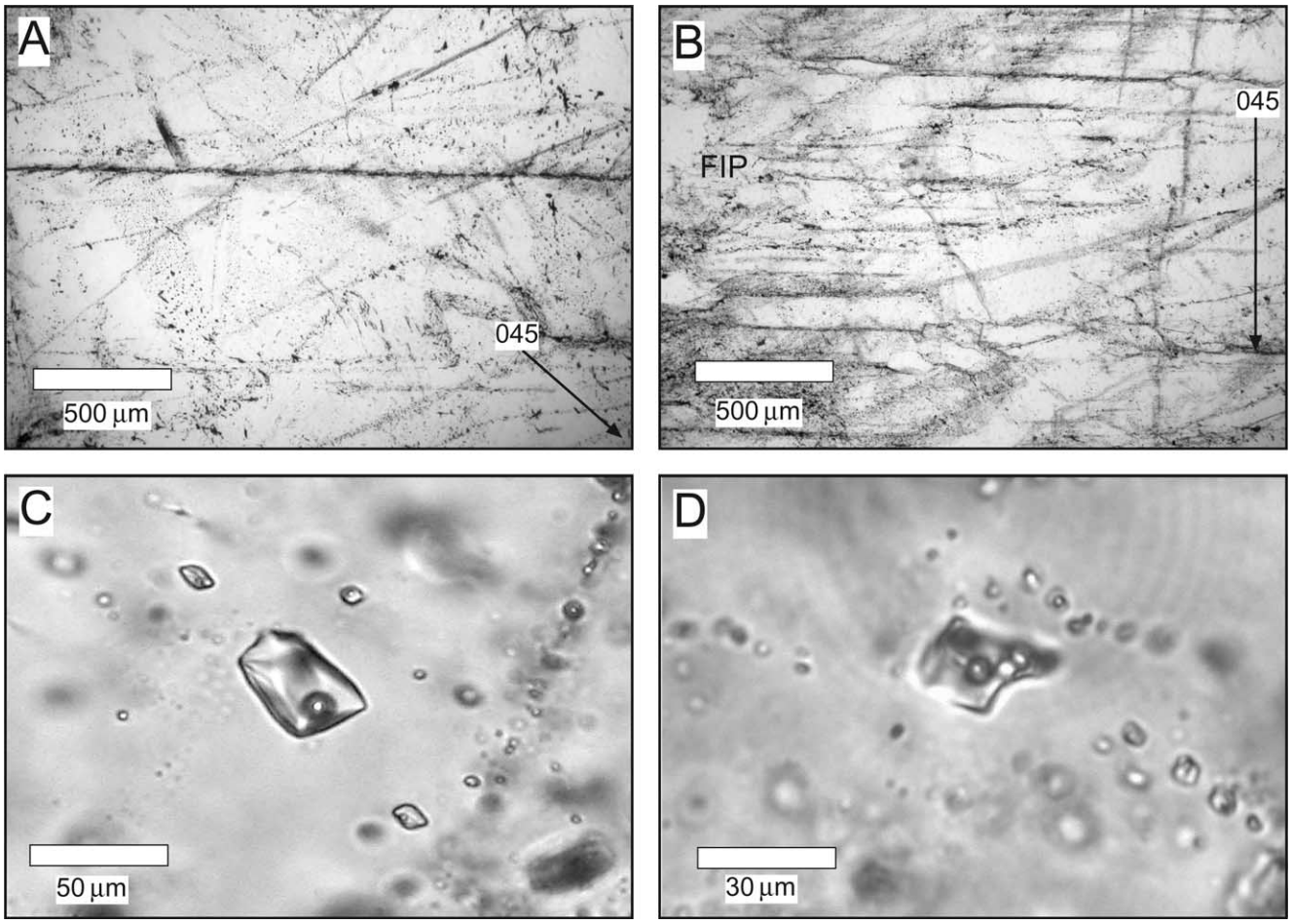

Fig. 10. Photomicrographs of sections used for microstructural analysis and fluid inclusion microthermometry: (A) sealed microfracture at an angle to FIP, section is horizontal and arrow indicates bearing of 045, (B) array of parallel FIP, section is horizontal and arrow indicates bearing of 045, (C) Type 1 two-phase liquid–vapour fluid inclusion, and (D) Type 2 three-phase liquid–vapour–solid fluid inclusion; the solid inclusion is a halite crystal.

been related to breccias formed during cataclasis (Sibson, 1986). The presence of a small volume of hydrothermal matrix mineralogy suggests that fluids also played a role in the brecciation process, though to what degree is uncertain as fluid expulsion is a response to pressure dissipation as the breccias are emplaced could result in a lesser volume of matrix (McCallum, 1985). When all these factors are taken into consideration we conclude that the brecciation mechanism involved in the formation of the biotite matrix breccias was a hybrid between two modes of breccia formation; cataclasis during shearing and hydraulic failure induced by elevated fluid pressures. These two processes have contributed to the formation of a breccia with low D_r^* values, low matrix to clast ratios, a hydrothermal mineralogy in the matrix, evidence of clast reworking and localisation at the sheared margin to the Poodla Granite.

Table 1
Summary of the two fluid inclusion type found in FIPs from syn-tectonic quartz veins

	Type 1	Type 2
Host mineral	Quartz	Quartz
Phases	L+V	L+V+S
Habit	Secondary/FIP	Secondary/FIP
T_m ice	−19.6/−25.1	−34.2/−43.8
wt% NaCl equivalent	22.4/26.1	35.0/45.6
T_h	170/209	217/246
N	54	31

The other style of brecciation present in the Telechie Valley (actinolite matrix breccias) have significantly different textural, spatial and fractal characteristics. Actinolite breccias, in general, have a gradational contact relationship with the surrounding host lithologies. They form exclusively in the Ethiudna psammopelite unit in the Telechie Valley (Fig. 2) mainly in dilational positions within the Telechie Valley shear zone. The gradational nature of the contact, whereby unbrecciated psammopelite grades to fractured rock, the fractures being filled with actinolite, to actinolite matrix breccia is suggestive of in-situ breccia development. This conclusion is supported by the angular to sub-angular nature of clasts within the breccias, absence of exotic clast types and the jigsaw textures observed at outcrop and thin-section scales.

Fractal analysis performed on the clasts found in two samples of actinolite matrix breccia (TV44 and TV46) further support their in-situ development. D_r^* values of 7.04 ± 0.46 and 7.97 ± 0.69 for samples TV44 and TV46, respectively, indicate (Fig. 7c and d) that fluid pressure and regional stress variations

played a role in the initiation of brecciation. The large D_r^* values for actinolite breccias, when compared with biotite breccias, suggests a lack of maturity in the brecciation process that occurred during actinolite breccia formation. This feature can be attributed to the in-situ development and lack of post-failure transport. The lower D_s values, 1.20 and 1.17 for TV44 and TV46, respectively, serve to highlight the lower degree of transport involved in the actinolite matrix breccia forming process in comparison with the degree of transport involved in the formation of the biotite matrix breccias. The two fractal dimensions and the lower clast to matrix ratios of the actinolite breccias suggest that an increase in fluid pressure is the key factor in the brecciation process.

8.2. Palaeostress orientations during shear zone formation

The results of micro- and macrostructural analysis of fractures and fabrics were combined in order to determine whether the palaeostress conditions during shear zone formation were favourable for the development of breccias. This method has been used to reconstruct palaeostress histories in granites in the Massif Central (Lespinasse and Cathelineau, 1990) and the Rhine graben (Ándre et al., 2001). Palaeostress conditions are often hard to establish from highly-strained ductily deformed rocks, largely due to the unknown amount of rotation of fabric elements within the sheared rocks. In this study, we have not tried to directly measure palaeostress, but have compared the implied stress directions and relative magnitudes from analysis of brittle fractures in quartz veins with the directions and relative magnitudes of principal strain vectors derived from fabric analysis of the shear zone. This analysis does not prove the stress state of the Mid/Upper Crust at the time of deformation, but it does allow an assessment of whether the shear zone, breccias and quartz veins are consistent with formation in the same stress field.

The dominant structures in the Telechie Valley shear zone are the result of shearing and compression during the D_3 phase of the Olarian Orogeny at 1579 ± 27 Ma constrained by electron microprobe analysis of monazite growing in association with D_3 fabric forming minerals (Clark et al., 2004). The orientations of fabrics, fractures and microfractures of samples from in and around the Telechie Valley allow a number of constraints to be placed on the orientations of the principal stress directions. The Andersonian model of faulting, which is based on a homogeneous stress state and the Coulomb failure criteria, predicts that the maximum principal compressive stress was between 30 and 45° to the plane of a shear zone at its inception (Anderson, 1942; Scholz, 1990). Shear planes within the shear zone indicate that the bulk shear plane strikes 039° and dips 84°SE. Lineations present on these surfaces plunge 55° towards 239° (Fig. 4c), defining the inferred vector of Olarian shear displacement. Sinistral movement indicators include sheared early pegmatites that form delta clasts (Fig. 5d) and show that the NW block moved down and SW relative to the SE block. Synthetic shear fractures in quartz veins strike 011° and dip 80°E (Fig. 9c), at a low angle to the shear plane (Fig. 4b). Antithetic fracture planes dip 86°NE with a strike of 116° (Fig. 4d), at a high angle to the shear plane. Axial planes of folds (S_3) in the more competent psammopelitic units strike 060° and dip relatively steeply (Fig. 4f) with fold axes (F_3), that plunge ~30° towards 060°. This orientation is consistent with the asymmetry of D_3 related folding throughout the Olary Domain (Clarke et al., 1986). The psammopelitic units form lenses within the shear zones and are interpreted as low-vorticity domains with the strain vectors approximating the regional D_3 stress vectors. The F_3 orientations in the less competent pelites have been rotated (Fig. 4e), due to higher vorticity shearing, towards the extension direction of the shear zone as defined by the mineral elongation lineations (Fig. 4c).

The D_3 deformation features recorded in the field allow an interpreted reconstruction of the relative stress field (Fig. 11). These structures indicate an approximately horizontal NNW–SSE compression axis, approximately parallel to the shortening axis for the folds in the low vorticity domains (Fig. 11). In this model, the minimum principal stress axis is oriented ENE–WSW with the intermediate principal stress orientation being near vertical. The relationships between the three principal stress orientations are consistent with the Andersonian stress state present within a strike slip regime.

The D_3 related quartz veins have an average strike of 140° and dip 75°S (Fig. 4g); this orientation aligns them approximately perpendicular to the shear zone boundary and at an angle of ca. 20° to the previously interpreted compression direction. Given the observation that quartz veins are: (1) restricted to the shear zone; (2) cut the high-vorticity shear zone fabric; (3) are relatively undeformed; and (4) preserve numerous microfractures, the veins are interpreted as forming towards the end of shearing. The veins are extensional features that, we interpret, opened perpendicular to the maximum principal stress axis (σ_1). This suggests that towards the end of shearing the stress field was perturbed and rotated ca. 20° anti-clockwise with respect to the shear zone (Fig. 11), perhaps due to block rotation of the shear zone or stress perturbation due to weakening and movement of the shear zone. Fluid inclusion planes (FIPs) within these quartz veins are approximately parallel to the orientation of the veins themselves and are interpreted to mark the maximum–intermediate principal stress plane, as would be expected for opening mode microfractures (Friedman, 1963; Engelder, 1974). Microfractures in the syn-tectonic quartz veins may also be correlated to the perturbed stress field present towards the end of D_3 shearing. Fig. 9b and c shows two orientations of microfractures that are at an angle of ca. 60° to each other. Within the inferred stress regime these can be interpreted as shear fractures, forming an apparent conjugate set. The orientations of the quartz veins (Fig. 4g) and FIP (Fig. 9d) with the interpreted rotated local D_3 stress field prevailing toward the end of shearing (Fig. 11) allows the microthermometric results obtained from fluid inclusions contained in the FIPs to constrain the PT conditions of fluid trapping during the late stages of D_3.

8.3. Fluid pressure controls on breccia formation

Data from this study, when combined with previous studies of the geology in the Telechie Valley (Skirrow et al.,

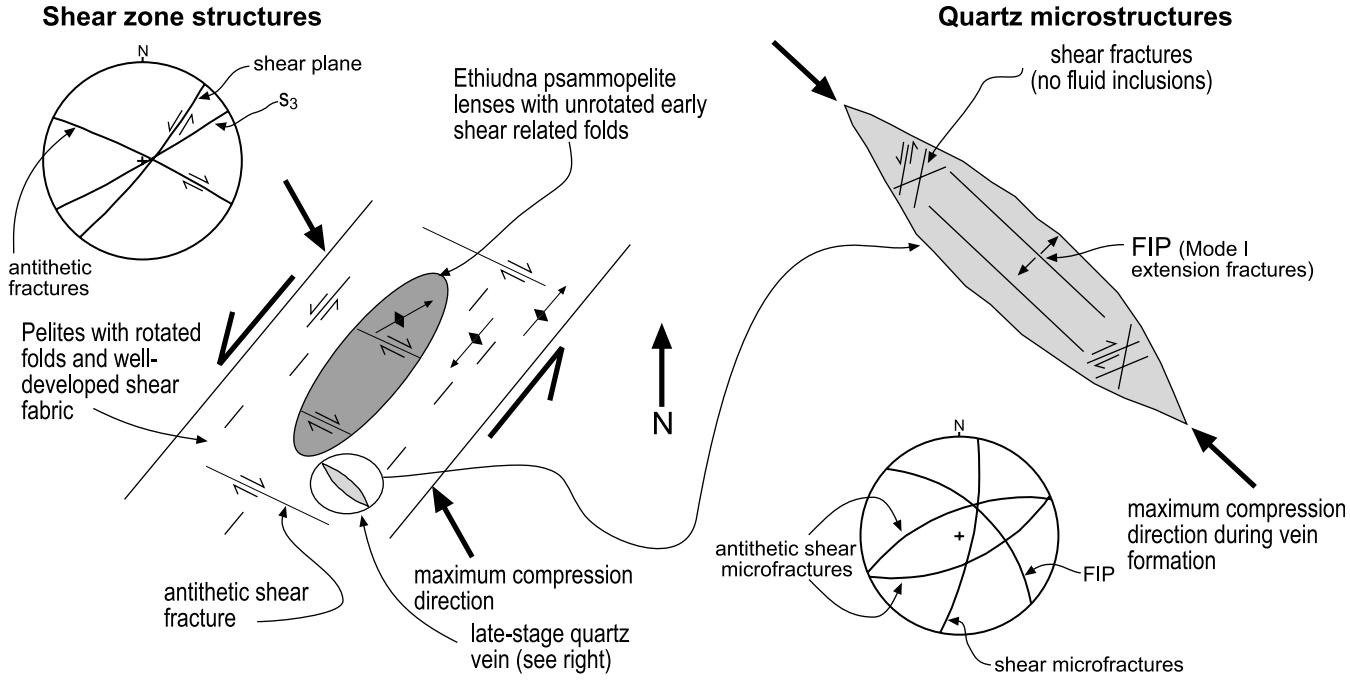

Fig. 11. Summary of the main field structural and microstructural relationships observed in the Telechie Valley shear zone and their relationship to the inferred stress field for D_3 related shearing. Note the apparent ca. 20° rotation of the inferred stress axes towards the end of shearing at the time of veining.

2000; Clark et al., 2004), provide good constraints for the general P–T–t conditions during shearing and brecciation. Temperatures during syn-tectonic vein formation in the Telechie Valley have been estimated from the application of oxygen isotope thermometry and have yielded values of 394–426 °C (Clark et al., 2004). The relatively high pressures recorded by the wall rocks (300–500 MPa (Clark et al., 2004)) indicate a deep structural level consistent with crustal thickening associated with Olarian Orogeny at the time of shear zone formation. The timing of shearing and fluid flow have been demonstrated to be synchronous. Monazite inclusions in biotite that define the main shear foliation yield an age of 1579±27 Ma (Clark et al., 2004) and U–Pb ages from the matrices of actinolite breccias yield ages of 1588–1583 Ma (Skirrow et al., 2000). These ages are consistent with Sm–Nd isotope ages of regional calcsilicate alteration of 1575±26 Ma (Kent et al., 2000).

Fractal analysis of the two styles of breccias present in the Telechie Valley indicates that variations in the fluid pressure magnitudes were the primary control on the brecciation process. In order to initiate hydraulic fracturing of the host rocks in the Telechie Valley two conditions must be achieved. First, there must be failure along the shear zone in order to create a space or dilatancy for the breccia to form and, second, the absolute magnitude of fluid pressure variance must be greater than the tensile strength of the wallrock. The variations in fluid pressure during shearing associated with brecciation can be deduced by determining the differences in the trapping conditions of the two types of fluid inclusions identified in this study. Isochores for the two fluids found in FIP related to shearing have been determined based on the calculated fluid densities and compositions (Fig. 12) from the FLUIDS package of programs (Bakker, 2003). As can be seen in Fig. 12, using the temperature of 400 °C deduced previously by stable isotope investigations (Clark et al., 2004), trapping of two-phase low salinity inclusions occurred at pressures of 380–420 MPa, which is equivalent to lithostatic fluid pressures expected at depths of 10–12 km. Assuming the same trapping temperature of 400 °C, three-phase inclusions yield trapping pressures of 220–290 MPa. This pressure, while greater than hydrostatic fluid pressures expected at this depth, is significantly lower than the trapping pressures recorded by the two-phase inclusions.

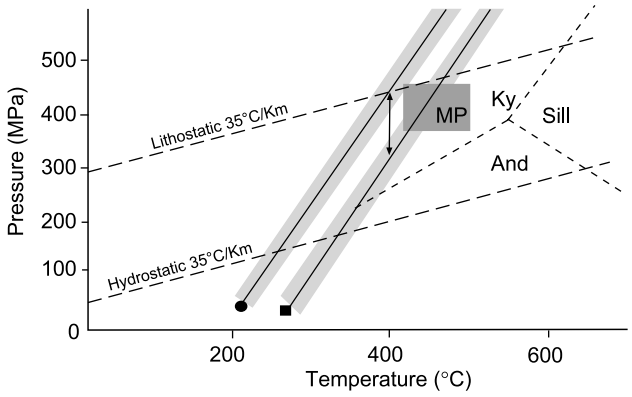

Fig. 12. PT reconstruction of the conditions in the host rocks during fluid inclusion trapping in the Telechie Valley shear zone. The circle and square represent homogenisation temperatures of Type 1 and Type 2 fluid inclusions, respectively. Ky: kyanite, Sill: sillimanite, And: andalusite, MP: peak metamorphic conditions for the Olary Domain from Flint and Parker (1993).

The difference between the trapping pressures of the two fluid inclusion types (Fig. 12) is consistent with previous models concerning the roles of fluids during brittle fracturing (Sibson, 1986, 1996). These changes indicate that cycling of pressure related to fault valve mechanisms may have been a contributing factor to failure within the shear zone. Failure on a fault at the depths (10–12 km) calculated for the Telechie Valley shear zone requires elevated pore fluid pressures to initiate failure. Streit and Cox (2001) estimated that the pore fluid pressures required to initiate failure in strike-slip regimes were near lithostatic at these depths. Evidence from fluid inclusions in this study suggests that near lithostatic fluid pressure conditions were achieved during D_3. Such high pore fluid pressure conditions may be generated in fault zones due to fault lithification and fluid trapping (Angevine et al., 1982; Sibson, 1990; Streit and Cox, 2001).

The two types of breccias present in the Telechie Valley can be directly related to the environment in which each breccia formed. Actinolite matrix breccias generally form in the central region of the shear zone (Fig. 13) and can be considered to form by the fluid induced implosion of wall rocks into dilatant sites along the shear zone. Dilatant sites were created during initial fault failure and are most likely related to irregularities in the geometry of the fault plane. Given the calculated magnitude of the pressure differences, ~100 MPa, and the tensile strength of wall rocks in general of ~50 MPa (Sibson, 1986), it is considered likely that fluid pressure fluctuations led to the failure of the wall rocks into the dilatant sites and the formation of actinolite matrix breccias. This type of failure is also reflected in the fractal values that suggest in-situ development and a lack of post-failure transport. Previous studies (Skirrow et al., 2000; Clark et al., 2005) of the chemistry of fluids related to shearing in the Telechie Valley are consistent with the precipitation of a hydrothermal, calcsilicate matrix mineralogy in the breccias within the shear zone.

In contrast to the actinolite matrix breccias, the biotite matrix breccias are found at the sheared contact between the granite and surrounding pelitic schists (Fig. 13). The high clast to matrix ratio and large degree of frictional attrition experienced by clasts indicate that fluctuations in the fluid pressure resulting from failure did not play a significant role in their generation.

9. Conclusions

This work shows that a detailed study of the structural setting, fractal characteristics and palaeofluids trapped as fluid inclusions associated with breccias can provide useful quantitative constraints on the physical conditions that lead to their formation. The main conclusions obtained from the study of the breccia systems in the Telechie Valley are:

(1) Breccias occur in structurally controlled positions in the Telechie Valley and structural control of these locations based on the reconstruction of the palaeostress orientations can be related to strike-slip failure along a Mesoproterozoic Olarian Orogeny shear zone. Shearing took place at depths of 10–12 km and temperatures of ~400 °C and was associated with elevated fluid pressures related to the metamorphic dehydration of the Willyama Supergroup (Clark et al., 2005).

(2) Two styles of breccias have been identified in the Telechie Valley based on matrix mineralogy, clast to matrix ratios and fractal characteristics. They are a biotite matrix breccia, which has a high clast to matrix ratio, low D_r^* and relatively high D_s^* values. These parameters suggest that tectonic comminution was a significant contributor in the generation of these breccias. Actinolite breccias have lower clast to matrix ratios, higher D_r^* and lower D_s^* values indicating that they formed in-situ with little subsequent transport. Brecciation occurred in dilatant sites along the fault plane and was largely dependent on fluctuations in fluid pressures associated with fault valving.

(3) The fluctuations in fluid pressure have been quantified by the analysis of structurally controlled syn-tectonic fluid

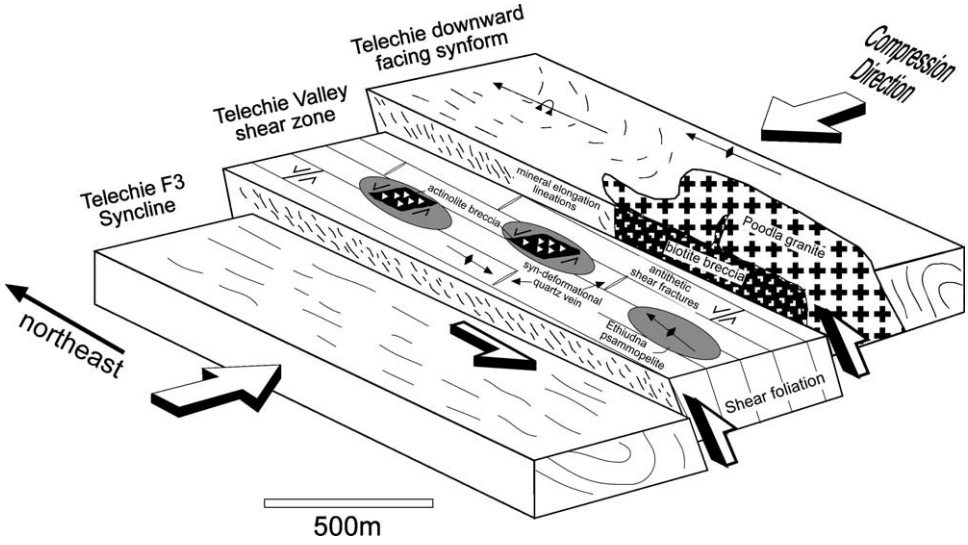

Fig. 13. Block diagram showing the geometry, kinematics and locations of brecciation styles within the Telechie Valley. Approximate compression direction refers to inferred stress state late in the evolution of the shear zone.

inclusions trapped in FIP that formed during shearing. Near lithostatic fluid pressures recorded by fluid inclusions led to failure along the fault. The resulting drop in fluid pressure led to failure of the wall rock into dilatant sites as the magnitude of the fluid pressure change exceeded the tensile strength of the wall rock.

Acknowledgements

This work is the result of work funded by ARC Linkage grant LP0347584 and is part of work towards a Ph.D. by CC. We gratefully acknowledge discussions with Colin Conor, Wolfgang Preiss, Alistair Crooks and Justin Payne about fluid related deformation processes and many other aspects of the geology of the Curnamona Province. Marc Lespinasse at UHP-Nancy is thanked for his help in demonstrating the method and relevance of FIP analysis. Nick Oliver, Michel Jébrak Jafar Hadizadeh, Anne-Marie Boullier and Tom Blenkinsop are thanked for constructive reviews.

References

Anderson, E.M., 1942. The Dynamics of Faulting and Dyke Formation with Applications to Britain. Oliver and Boyd, Edinburgh. 234pp.

Ándre, A.-S., Sausse, J., Lespinasse, M., 2001. New approach to the quantification of palaeostress magnitudes: application to the Soultz vein system (Rhine graben, France). Tectonophysics 336, 215–231.

Angevine, C.L., Turcotte, D.L., Furnish, M.D., 1982. Pressure solution lithification as a mechanism for the stick-slip behavior of faults. Tectonics 1-2, 151–160.

Archibald, N., 1980. Toraminga Valley outcrop geology (map). In: Esso Australia Ltd, Plumbago EL 450. South Australian Department of Primary Industries and Resources. Open file Envelope, 3447 (unpublished).

Ashley, P.M., Cook, N.D.J. & Fanning, C.M. 1996. Geochemistry and age of metamorphosed felsic igneous rocks with A-type affinities in the Willyama Supergroup, Olary Block, South Australia, and implications for mineral exploration. Lithos 38(3–4), 167–184.

Bakker, R.J., 2003. Package FLUIDS; 1. Computer programs for analysis of fluid inclusion data and for modelling bulk fluid properties. Chemical Geology 194, 3–23.

Bell, T.H. 1978. Progressive deformation and reorientation of fold axes in a ductile mylonite zone; the Woodroffe Thrust. Tectonophysics 44, 285–320.

Berubé, D., Jébrak, M., 1999. High precision boundary fractal analysis for shape characterization. Computers and Geosciences 25, 1059–1071.

Bierlein, F.P., Ashley, P.M., Plimer, I.R., 1995. Sulphide mineralisation in the Olary Block, South Australia: evidence for syn-tectonic to late-stage mobilisation. Mineralium Deposita 30, 424–438.

Bjørnerud, M.G., 1998. Superimposed deformation in seconds: breccias from the impact structure at Kentland, Indiana (USA). Tectonophysics 290, 259–269.

Blenkinsop, T.G., 1991. Cataclasis and processes of particle size reduction. Pure and Applied Geophysics 136, 59–86.

Burnham, C.W., 1985. Energy-release in subvolcanic environments: implications for breccia formation. Economic Geology 80, 1515–1522.

Carreras, J., Druguet, E. & Griera, A. 2005. Shear zone-related folds. Journal of Structural Geology 27, 1229–1251.

Clark, C., James, P., 2003. Hydrothermal brecciation due to fluid pressure fluctuations: examples from the Olary Domain, South Australia. Tectonophysics 366, 187–206.

Clark, C., Schmidt Mumm, A., Faure, K., 2005. Timing and nature of fluid flow during Mesoproterozoic shear zone formation, Olary Domain, South Australia. Journal of Metamorphic Geology 23, 147–164.

Clarke, G., Burg, J., Wilson, C., 1986. Stratigraphic and structural constraints on the Proterozoic tectonic history of the Olary Block, South Australia. Precambrian Research 34, 107–137.

Clarke, G., Guiraud, M., Wilson, C., Burg, J., 1987. Metamorphism in the Olary Block, South Australia; compression with cooling in a Proterozoic fold belt. Journal of Metamorphic Geology 5, 291–306.

Conor, C.H.H., 2003. Geology of the Olary Domain, Curnamona Province, South Australia. South Australia Department of Primary Industries and Resources Report Book, 2003/10.

Cook, N., Ashley, P., 1992. Meta-evaporite sequence, exhalative chemical sediments and associated rocks in the Proterozoic Willyama Supergroup, South Australia: implications for metallogenesis. Precambrian Research 56, 211–226.

Cook, N.D.F., Ashley, P.M. & Fanning, C.M. 1994. New geochronological results from the Willyama Supergroup, Olary Block, South Australia. In: Australian Research on Ore Genesis Symposium. Australian Mineral Foundation, Adelaide. (19.1–19.5).

Cox, S.F., Knackstedt, M.A., Braun, J., 2001. Principles of structural control on permeability and fluid flow in hydrothermal systems. In: Richards, J., Tosdal, R. (Eds.), Deformation, Fluid Flow and Ore Deposits. Society of Economic Geologists Short Course Proceedings 14, pp. 1–24.

Crooks, A.F., Webb, G., 2003. A metamorphic investigation of the Palaeoproterozoic metasediments of the Willyama Inliers, southern Curnamona Province, South Australia. Results from literature review, fieldwork, petrography, and the spatial distribution of metamorphic minerals. South Australia Department of Primary Industries and Resources Report Book, 2003/11.

Engelder, J.T., 1974. Cataclasis and the generation of fault gouge. Geological Society of America Bulletin 85, 1515–1522.

Etheridge, M.A., 1983. Differential stress magnitudes during regional deformation and metamorphism—upper bound imposed by tensile fracturing. Geology 11, 231–234.

Flint, D., Parker, A., 1993. Willyama inliers. In: Drexel, J., Preiss, W., Parker, A. (Eds.), The Geology of South Australia Geological Survey of South Australia Bulletin 54, pp. 82–93.

Friedman, M., 1963. Petrofabric of experimentally deformed calcite-cemented sandstones. Journal of Geology 21, 12–37.

Genna, A., Jébrak, M., Marcoux, E., Milesi, J., 1996. Genesis of cockade breccias in the tectonic evolution of the Cirotan epithermal gold system, West Java. Canadian Journal of Earth Sciences 33, 93–102.

Gibson, G.M., Nutman, A.P., 2004. Detachment faulting and bimodal magmatism in the Palaeoproterozoic Willyama Supergroup, south-central Australia; keys to recognition of a multiply deformed Precambrian metamorphic core complex. Journal of the Geological Society of London 161, 55–66.

Goldstein, R.H., Reynolds, T.J., 1994. Systematics of Fluid Inclusions in Diagenetic Minerals: SEPM Short Course 31. Society of Sedimentary Geology, Tulsa, OK, USA.

Jébrak, M., 1997. Hydrothermal breccias in vein-type ore deposits: a review of mechanisms, morphology and size distribution. Ore Geology Reviews 12, 111–134.

Kerrich, R., Allison, I., 1978. Vein geometry and hydrostatics during Yellowknife mineralisation. Canadian Journal of Earth Sciences 15, 1523–1543.

Kent, A.J.R., Ashley, P.M., Fanning, C.M., 2000. Metasomatic alteration associated with regional metamorphism; an example from the Willyama Supergroup, South Australia. Lithos 54, 33–62.

Laznicka, P., 1988. Breccias and Coarse Fragmentites. Petrology, Environments, Associations, Ores. Elsevier, Amsterdam.

Lespinasse, M., Cathelineau, M., 1990. Fluid percolations in a fault zone: a study of fluid inclusion planes (FIP) data. Journal of Geophysical Research 184, 173–187.

Lorilleux, G., Jébrak, M., Cuney, M., Baudemont, D., 2002. Polyphase hydrothermal breccias associated with unconformity-related uranium mineralisation (Canada): from fractal analysis to structural significance. Journal of Structural Geology 24, 323–338.

Lu, J., Plimer, I.R., Foster, D.A., Lottermoser, B.G., 1996. Multiple post-orogenic reactivation in the Olary Block, South Australia: evidence from $^{40}Ar/^{39}Ar$ dating of pegmatitic muscovite. International Geological Revenue 38, 665–668.

McCallum, M.E., 1985. Experimental evidence for fluidization processes in breccia pipe formation. Economic Geology 80, 1523–1543.

Oliver, N.H.S., Ord, A., Valenta, R.K., Upton, P., 2001. The role of rock rheological heterogeneity in fluid flow and ore genesis with examples and numerical models from the Mt Isa District. In: Richards, J., Tosdal, R. (Eds.), Deformation, Fluid Flow and Ore Deposits. Society of Economic Geologists Short Course Proceedings 14,, pp. 51–74.

Oliver, N.H.S., Valenta, R.K., Wall, V.J., 1990. The effect of heterogeneous stress and strain on metamorphic fluid-flow, Mary-Kathleen, Australia, and a model for large-scale fluid circulation. Journal of Metamorphic Geology 8, 311–331.

Ord, A., Oliver, N.H.S., 1997. Mechanical controls on fluid flow during regional metamorphism: some numerical models. Journal of Metamorphic Geology 15, 345–359.

Page, R.W., Stevens, B.J.P., Gibson, G.M., Conor, C.H.H., 2000. Geochronology of Willyama Supergroup rocks between Olary and Broken Hill, and comparison to northern Australia. Geoscience Australia Record 2003/10, 72–75.

Paul, E., Sandiford, M., Flöttman, T., 2000. Structural geometry of a thick-skinned fold-thrust belt termination; the Olary Block in the Adelaide Fold Belt, South Australia. Australian Journal of Earth Sciences 47, 281–289.

Payne, J.L., 2003. Geochemical constraints on the alteration of the Poodla Granite, Olary Domain, South Australia. BSc (Hons) thesis, University of Adelaide.

Reeve, J.S., Cross, K.C., Smith, R.N., Oreskes, N., 1990. Olympic Dam copper–uranium–gold–silver deposit. In: Hughes, F. (Ed.), Geology of the Mineral Deposits of Australia and Papua New Guinea: Volume 2. Australasian Institute of Mining and Metallurgy, pp. 1009–1035.

Ridley, J. 1993. The Relations between Mean Rock Stress and Fluid-Flow in the Crust - with Reference to Vein-Style and Lode-Style Gold Deposits. Ore Geology Reviews 8, 23–37.

Robertson, R., Preiss, W., Crooks, A., Hill, P., Sheard, M., 1998. Review of the Proterozoic geology and mineral potential of the Curnamona Province in South Australia. AGSO Journal of Australian Geology and Geophysics 17, 169–182.

Roedder, E., 1984. Fluid Inclusions, Reviews in Mineralogy 12. Mineralogical Society of America. 644pp.

Scholz, C.H., 1990. The Mechanics of Earthquakes and Faulting. Cambridge University Press. 439pp.

Sibson, R.H., 1986. Brecciation processes in fault zones: inferences from earthquake rupturing. Pure and Applied Geophysics 124, 159–174.

Sibson, R.H., 1990. Conditions for fault-valve behaviour. In: Knipe, R.J., Rutter, E.H. (Eds.), Deformation Mechanisms, Rheology and Tectonics. Geological Society, London, Special Publications 54, pp. 15–28.

Sibson, R.H., 1996. Structural permeability of fluid-driven fault-fracture meshes. Journal of Structural Geology 18, 1031–1042.

Skirrow, R.G., Ashley, P.M., 2000. Proterozoic Cu–Au systems of the Curnamona Province—members of a global family? MESA Journal 19, 48–50.

Skirrow, R.G., Ashley, P.M., McNaughton, N.J., Suzuki, K., 2000. Time–space framework of Cu–Au(–Mo) and regional alteration systems in the Curnamona Province. Geoscience Australia Record 2003/10, 22–25.

Streit, J.E., Cox, S.F., 2001. Fluid pressures at hypocenters of moderate to large earthquakes. Journal of Geophysical Research 106, 2235–2243.

Turcotte, D.L., 1986. Fractals and fragmentation. Journal of Geophysical Research 91, 1921–1926.

Valenta, R.K., Cartwright, I., Oliver, N.H.S., 1994. Structurally controlled fluid-flow associated with breccia vein formation. Journal of Metamorphic Geology 12, 197–206.

Yanattieva, O.K., 1946. Solubility polytherms in the system $CaCl_2$–$MgCl_2$–H_2O and $CaCl_2$–NaCl–H_2O. Zhurnal Prikladnox Khimii 19, 709–722.

Yang, K., Ashley, P., 1994. Stratabound Breccias in the Willyama Supergroup, Olary Block, South Australia Australian Research on Ore Genesis Symposium. Australian Mineral Foundation, Adelaide, pp. 16.1–16.5.